The Pennsylvania State University
The Graduate School
College of Earth and Mineral Sciences

CORRECTING $\delta^{13}CH_4$ ANALYSES FOR KRYPTON INTERFERENCE: THE POTENTIAL IMPACT ON METHANE BUDGET STUDIES

A Thesis in
Geosciences
by
Emily A. Doyle

Submitted in Partial Fulfillment
of the Requirements
for the Degree of

Master of Science

May 2017

The thesis Emily A. Doyle was reviewed and approved* by the following:

Richard B. Alley
Evan Pugh Professor of Geosciences
Thesis Adviser

Katherine H. Freeman
Evan Pugh Professor of Geosciences

Lee R. Kump
Professor of Geosciences
Head of the Department of Geosciences

Demian M. Saffer
Professor of Geosciences
Associate Head for Graduate Programs and Research of the Department of Geosciences

* Signatures will be on file in the Graduate School

ABSTRACT

Methane (CH_4) enters the atmosphere through numerous sources, each with a unique carbon and hydrogen isotope signature ($\delta^{13}CH_4$ and $\delta D(CH_4)$, respectively). Methane budget studies use atmospheric CH_4, $\delta^{13}CH_4$, and $\delta D(CH_4)$ records to constrain methane sources over time. However, previous studies found that krypton (Kr) interferes with $\delta^{13}CH_4$ values when measured via continuous flow isotope-ratio mass spectrometry (CF-IRMS). To account for this interference, we determined a Kr correction for the methane analytical system at The Pennsylvania State University (PSU). We measured this correction by adding an additional gas chromatography (GC) column to the preconcentration unit, which separated the Kr and CH_4 peaks. By measuring three standards with both the original and modified systems, we quantified the Kr correction as a function of $1/[CH_4]$ and applied it to previously published methane budgets. The Kr correction ranged from 0 to -0.4 ± 0.4‰. We used a simple two-box model to determine how this correction affected estimated methane emissions from biomass burning (BMB) and biogenic sources. Overall, the Kr correction equally decreased reconstructed BMB emissions and increased biogenic emissions, and the size of this shift differed between hemispheres. In the Southern Hemisphere, the maximum shift in emissions was 0.4 ± 0.5 Tg/year; in the Northern Hemisphere, the maximum shift was 1.5 ± 1.6 Tg/year. In all cases, the corrected budgets were indistinguishable from the originals within the combined measurement and computational uncertainties. However, Kr interference may be greater for other CF-IRMS systems and should be considered in future $\delta^{13}CH_4$ analyses.

TABLE OF CONTENTS

List of Figures

List of Tables

CHAPTER ONE

Introduction

Methane (CH_4) is one of the most abundant greenhouse gases in today's atmosphere and has a marked impact on Earth's climate. Since the mid-19th century, the atmospheric concentration of methane has more than doubled because of increased anthropogenic emissions[4–11]. This rise accounts for 17% of the increase in radiative forcing over the past 250 years[12]. Because methane has a significant role in climate forcing, it is important to monitor methane emissions from both anthropogenic and natural sources. Different sources release methane with different carbon and hydrogen isotopic compositions[13–16]. Because we know the isotopic signals of methane's major sources, we can analyze isotopic records of atmospheric methane to determine how these sources have changed over time[2–4,16,17]

However, Schmitt et al.[1] identified a potential error in prior studies of $\delta^{13}CH_4$ (also called methane budget studies). A standard analytical technique for measuring $\delta^{13}CH_4$, continuous flow isotope-ratio mass spectrometry (CF-IRMS), may not completely separate krypton (Kr) from CH_4. The degree of peak overlap is proportional to the mixing ratio of methane ($[CH_4]$) and is specific to each analytical system (IRMS and the preconcentration unit). For some systems, Kr falsely enriches $\delta^{13}CH_4$ measurements by up to ~2.38‰[1]. This paper addresses the Kr correction for The Pennsylvania State University's (PSU) analytical system, and how it affects our interpretation of CH_4 sources over time.

CHAPTER TWO

Background

2.1 Previous Methane Budget Studies

Methane budget models use data from several sources, including direct air sampling, satellite observations, and ice core gas records[4,10,11]. Ice cores are essential to atmospheric reconstructions because they contain direct samples of atmospheric air beyond the instrumental record. As snow densifies to ice, it traps small bubbles of air, which are advected deeper into the ice sheet. By extracting and analyzing these bubbles, we can reconstruct atmospheric [CH_4] back to 800 ka[8].

Methane enters the atmosphere from geologic, biogenic, and pyrogenic sources, each with a distinct $\delta^{13}C$ signature. Geologic sources (mean of -38 ± 7‰) include volcanic emissions and hydrocarbon seeps; biogenic sources (mean of -60 ± 5‰) include wetlands, ruminants, and rice paddies; and pyrogenic sources (mean of -22 ± 3‰) include natural and anthropogenic biomass burning (BMB) and coal burning[3,13–15,18,19]. The primary sink of atmospheric methane is reaction with hydroxyl radicals (OH) in the troposphere, which removes methane via oxidation[19]. By using source $\delta^{13}C$ values and atmospheric records of [CH_4] and $\delta^{13}CH_4$, models can accurately constrain estimates of methane sources and sinks over time. Many methane budget studies focus on the Holocene Epoch, and particularly on how anthropogenic and natural methane emissions have changed in the last 2 ky[2,3,16,17].

This paper focuses on methane budgets by Sapart et al.[2], Mischler et al.[3], and Sowers[4], who used $\delta^{13}CH_4$ data measured at PSU. To estimate methane source emissions, each study used an atmospheric box model derived from that in Tans[20]. They used additional proxies to support

their results, e.g., the Northern Hemisphere charcoal index and reconstructed records of temperature, precipitation, and deforestation rates.

Sapart et al.[2] constrained methane emissions for the past 2 ky, using $\delta^{13}CH_4$ data from two Greenland ice cores. They grouped methane sources into four categories: biogenic, pyrogenic, geologic, and fossil fuels. To invert for all sources, Sapart et al.[2] used background scenarios from the existing literature to constrain the model. They reported three excursions in $\delta^{13}CH_4$ between 0 and 1600 CE (Fig. 1).

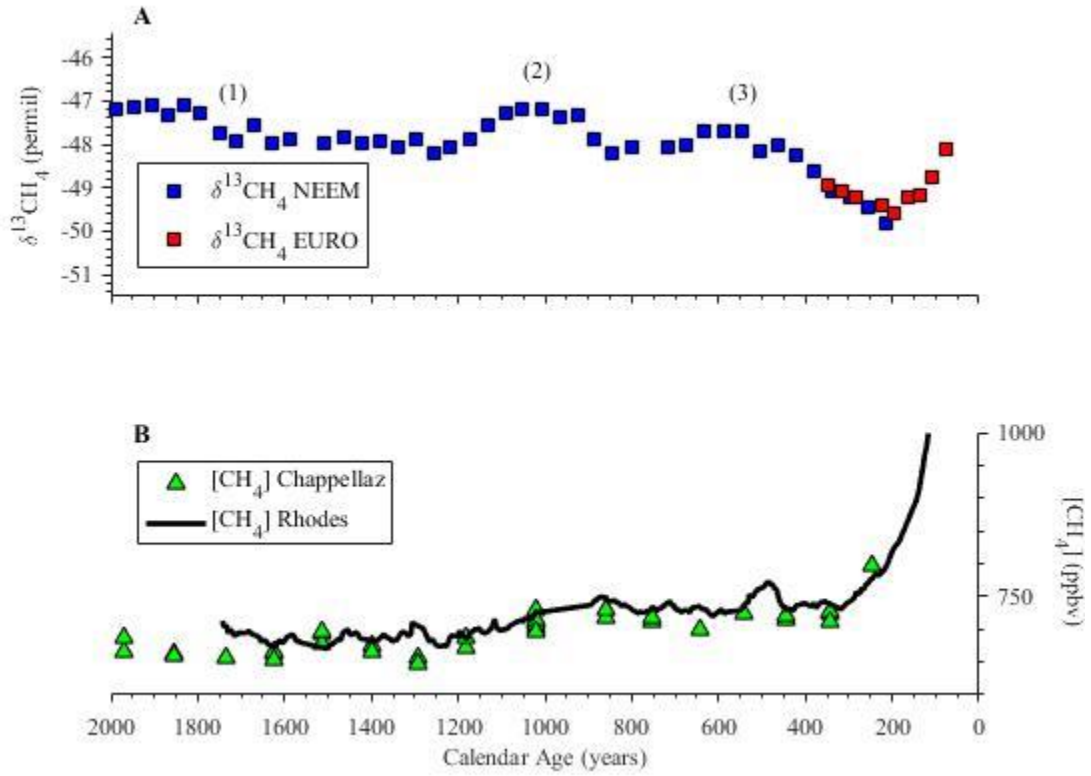

Figure 1. Sapart et al.'s[2] original $\delta^{13}CH_4$ record (A) and two $[CH_4]$ records (B) for the past 2 ky. Sapart et al.[2] data are from the NEEM (North Greenland Eemian Ice Drilling project) and EUROCORE ice cores. The $\delta^{13}CH_4$ record shows three primary excursions that Sapart et al.[2] attributed to (1) the fall of the Roman Empire and Han Dynasty, (2) the Medieval Climate Anomaly, and (3) The Little Ice Age. $[CH_4]$ data from Chappellaz et al.[7] and Rhodes et al.[10] are from the GRIP (Greenland Ice Core Project) and NEEM ice core, respectively.

During the first excursion (0-200 CE), $\delta^{13}CH_4$ decreased by ~1‰ with no clear change in [CH_4]. Sapart et al.[2] attributed this excursion to a drop in BMB after the fall of the Roman Empire and Han Dynasty. The second excursion (800-1200 CE) coincided with the Medieval Climate Anomaly (MCA) and showed a ~1‰ shift toward heavier methane sources. Sapart et al.[2] concluded that warmer temperatures caused extended droughts, which decreased biogenic emissions and increased natural fires. Concurrently, larger populations increased the amount of anthropogenic BMB and led to an overall ~50 ppbv increase in [CH_4][6]. Lastly, Sapart et al.[2] attributed the third excursion (1400-1600 CE), a ~1‰ increase in $\delta^{13}CH_4$, to colder temperatures during the Little Ice Age (LIA). They proposed that lower temperatures decreased biogenic emissions and reduced precipitation, which increased emissions from natural fires. Further, though [CH_4] increased by ~50 ppbv between 1400 and 1500 CE, it returned to its previous level by 1600 CE[6]. This [CH_4] spike supported Sapart et al.'s[2] hypothesis that deforestation increased during this time; however, the rapid drop in [CH_4] after 1500 CE was likely caused by a decline in population due to the unfavorable climate.

Mischler et al.[3] constructed a methane budget for the past 1 ky from the West Antarctic Ice Sheet (WAIS) ice core. Like Sapart et al.[2], Mischler et al.[3] found centennial scale variations in $\delta^{13}CH_4$ (Fig. 2). They also measured $\delta D(CH_4)$ to further constrain their model. Instead of an inversion technique, Mischler et al.[3] averaged data across three time slices (990-1460, 1460-1575, and 1589-1730 CE) and estimated source strengths during these periods. Overall, Mischler et al.[3] observed a gradual increase in agricultural emissions over the past 1 ky. This increase scaled with population growth and accounted for much of the gradual rise in [CH_4] during that time[7]. They also noted a decrease in BMB emissions and a sudden ~20 Tg/year drop in total [CH_4] emissions from 1500-1700 CE. Mischler et al.[3] agreed with previous studies[16] that these

signals were caused by European contact with the Americas and the decimation of the Native American population.

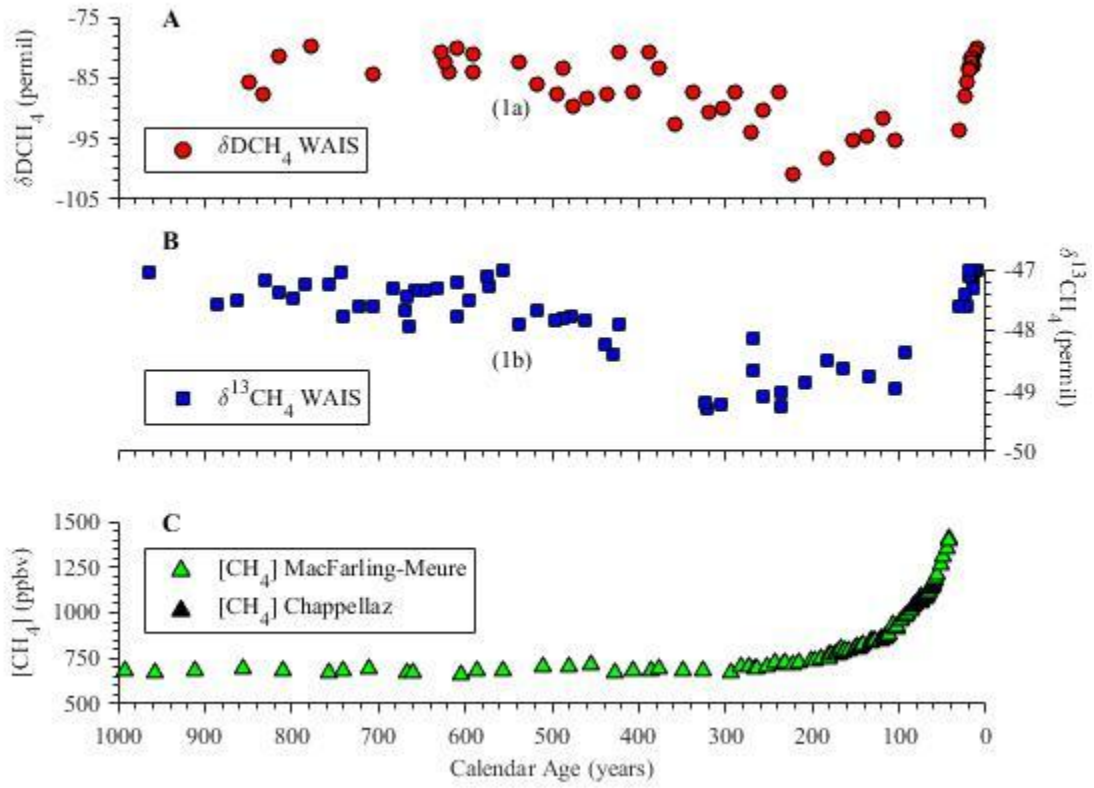

Figure 2. Mischler et al.'s[3] original $\delta^{13}CH_4$ (A) and $\delta D(CH_4)$ (B) records, and two $[CH_4]$ records for the past 1 ky (C). Mischler et al.[3] data are from the WAIS (West Antarctic Ice Sheet) ice core. Mischler et al.[3] attributed the ~2‰ decrease in $\delta^{13}CH_4$ (1a) and ~10‰ decrease in $\delta D(CH_4)$ (1b) to the decimation of the Native American population after European contact with the Americas. $[CH_4]$ data from MacFarling-Meure et al.[9] and Chappellaz et al.[7] are from the Law Dome and Byrd ice core, respectively.

On a longer timescale, Sowers[4] observed millennial scale variations in $\delta^{13}CH_4$ and $\delta D(CH_4)$ throughout the Holocene (Fig. 3). Between 10 ka and 4 ka, $\delta^{13}CH_4$ decreased while $\delta D(CH_4)$ remained relatively stable. Sowers[4] attributed these changes to natural causes, such as the activation of Arctic lakes ($\delta^{13}CH_4$ = -70‰; $\delta D(CH_4)$ = -390‰)[21] and the proliferation of C3 plants in wetlands ($\delta^{13}CH_4$ = -25‰)[22]. After 4 ka, however, $\delta^{13}CH_4$ stabilized and $\delta D(CH_4)$

began to increase, which he interpreted as the gradual release of methane from marine clathrates ($\delta^{13}CH_4$ = -60‰; $\delta D(CH_4)$ = -186‰)[23].

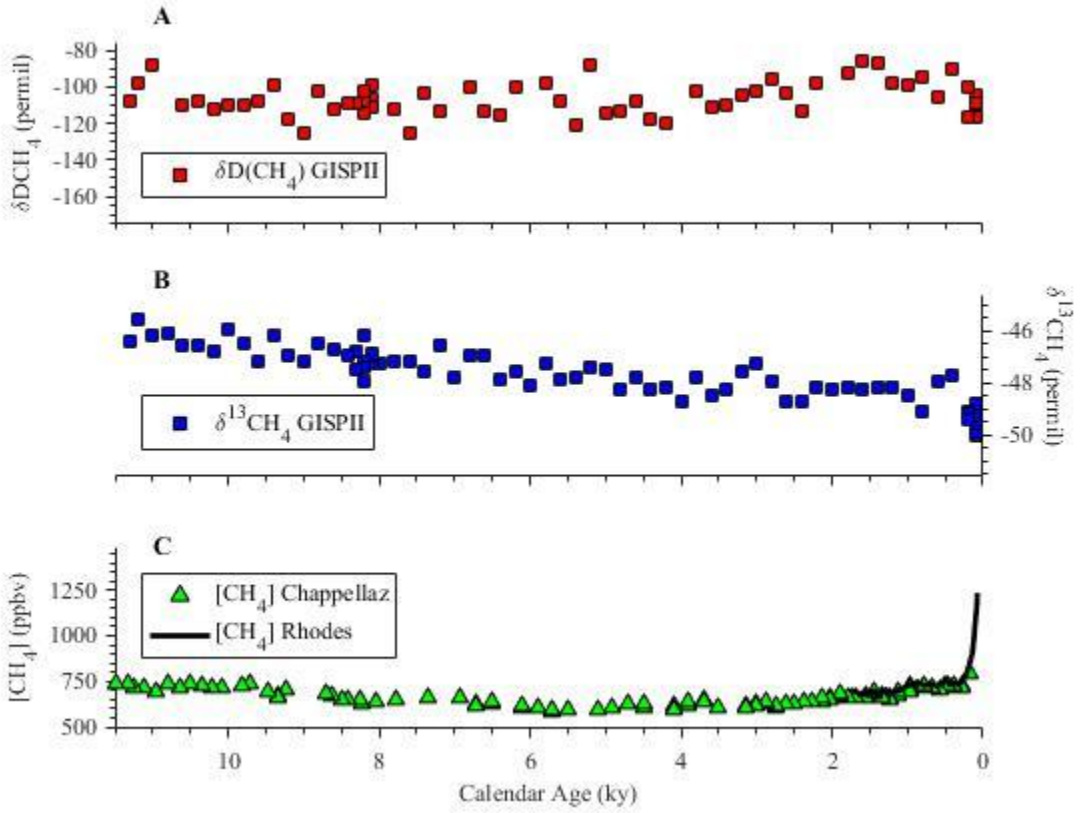

Figure 3. Sowers'[4] original $\delta^{13}CH_4$ (A) and $\delta D(CH_4)$ (B) records, and two $[CH_4]$ records over the past 10 ky (C). Sowers[4] data are from the GRIP II (Greenland Ice Core Project) ice core and show two shifts in methane sources: 1) From 10-4 ka, increased emissions from Arctic lakes and C3 plants decreased $\delta^{13}CH_4$ while $\delta D(CH_4)$ remained stable, and 2) from 4-1 ka, emissions from marine clathrates increased $\delta D(CH_4)$ while $\delta^{13}CH_4$ remained stable. Methane data from Chappellaz[7] and Rhodes[10] are from the NEEM (Northern Greenland Eemian Ice Drilling Project) and GRIP (Greenland Ice Core Project) ice core, respectively.

However, Sapart et al.[2], Mischler et al.[3], and Sowers[4] all used $\delta^{13}CH_4$ data from PSU, which were not then corrected for Kr interference. As such, their $\delta^{13}CH_4$ measurements were falsely enriched by a small offset that varied with $[CH_4]$ over time. To correct for this error, we have quantified the PSU's Kr interference, and herein revise the $\delta^{13}CH_4$ records from these

studies. We use a two-box model to reconstruct methane source emissions from both the original and the corrected datasets. Finally, we compare these reconstructions to determine if and how Kr interference affected the methane budget studies of Sapart et al.[2], Mischler et al.[3], and Sowers[4].

2.2 Carbon Isotope Analysis and the Krypton Interference

Continuous flow isotope-ratio mass spectrometry (CF-IRMS) is a primary technique for measuring $\delta^{13}CH_4$. Before entering the IRMS, CH_4 is converted to carbon dioxide (CO_2), with isotopologues of mass 44, 45, and 46. These molecules gain a single charge in the ion source, and they are detected in Faraday cups with their respective mass/charge ratio (m/z). The predominant signal enters the m/z 44 cup, but the less common isotopologues are also detected. These signals are integrated over time to measure $\delta^{13}CH_4$.

The CF-IRMS method assumes that Kr is separated from CH_4 before the sample enters the ion source. However, Schmitt et al.[1] showed that a standard CF-IRMS system does not achieve adequate separation, and that the $^{86}Kr^{2+}$ signal (m/z 43) also enters cups m/z 44, m/z 45, and m/z 46. This interference likely arises from multiple scattering processes as well as interactions within the flight tube. As a result, the lateral tail of the $^{86}Kr^{2+}$ signal falls into the m/z 44 cup and partially into the m/z 45 cup. Further, scattering of $^{86}Kr^{+}$ may produce a broad signal that affects cups m/z 45 and m/z 46. The amount of Kr interference depends on source settings, focusing parameters, and other factors unique to each analytical system. Schmitt et al.[1] measured Kr interference at The University of Bern, the Alfred Wegner Institute (AWI), and Institute for Marine and Atmospheric research Utrecht (IMAU) and found that Kr can enrich $\delta^{13}CH_4$ measurements by up to 2.38‰. They also identified peak overlap in PSU's system but did not determine a correction.

For a detailed description of Kr interference processes and how they affect $\delta^{13}CH_4$, see Schmitt et al.[1].

2.3 PSU's Analytical System and Potential Kr Interference

PSU's CF-IRMS system was detailed in Sowers et al.[24]. In summary, the system involves four steps: (1) preconcentration, (2) separation, (3) combustion, and (4) detection. During preconcentration, water, CO_2, and nitrous oxide (N_2O) are removed from the sample, and CH_4 is cryofocused. CH_4 is then separated from other trace impurities on a carbon Porous Layer Open Tubular (PLOT) gas chromatography (GC) column. The CH_4 effluent is quantitatively combusted to CO_2 before entering the ion source of the IRMS. Lastly, the three major isotopologues of CO_2 (m/z 44, m/z 45, m/z 46) are detected and integrated to determine $\delta^{13}CH_4$. With this system, Kr elutes 3.9 seconds after CH_4, and each peak has a width of ~2 seconds, causing peak overlap.

2.4 Correcting for Krypton Interference

Schmitt et al.[1] described several techniques to minimize Kr interference during analysis or correct for it afterward. To prevent Kr interference, the preconcentration unit must separate Kr from CH_4 before the sample enters the ion source. Kr and CH_4 have similar physicochemical properties and are, therefore, difficult to separate on a GC column at ambient temperatures[1]. However, a GC column or cryogenic trap easily separates Kr from the CO_2 sample peak after combustion[25]. With this modification, Kr elutes before the sample peak and does not interfere with the $\delta^{13}CH_4$ measurement. Schmitt et al.[1] also described several methods to correct for Kr interference post $\delta^{13}CH_4$ analysis. Early peak cut-off, for example, can eliminate 90% of the Kr

peak, but it also removes up to 10% of the CH_4 peak. One of the most accurate techniques is a time series correction, but it requires the raw beam data file. For a detailed discussion of correction methods and their advantages and disadvantages, see Schmitt et al.[1].

Another way to quantify the Kr correction is a graphing technique, which capitalizes on the linear relationship between Kr and CH_4. Schmitt et al.[1] used both this method and the time series correction method to quantify AWI's Kr correction. Both methods returned the same result within error. At PSU, we used the graphing technique to determine the Kr correction for our CF-IRMS system. By analyzing standards with our original preconcentration unit as well as a modified version, we determined the Kr correction as a function of $1/[CH_4]$. See Methods section for more details.

CHAPTER THREE

Methods

3.1 Analytical Methods

3.1.1 PSU's Original CF-IRMS System and New Modifications

The original CF-IRMS system was detailed in Sowers et al.[24]. It consisted of a preconcentration unit with a GC column, coupled to a MAT 252 mass spectrometer. To minimize Kr interference, an additional 8 m of carbon PLOT column were inserted after the combustion chamber. All other instrument settings remained unchanged (Fig. 4).

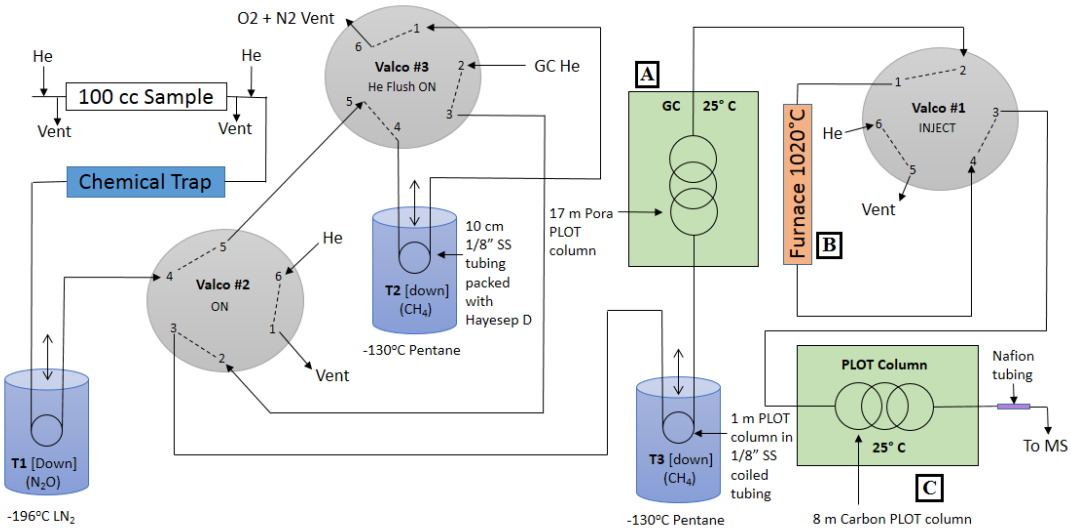

Figure 4. PSU's modified preconcentration unit, showing the original GC column (A), the combustion furnace (B), and the additional PLOT column (C). Modified from Sowers[24].

3.1.2. Standards

Three standards (A, B, C) with known methane concentrations were analyzed on both the original and modified PSU systems. Standards A, B, and C had CH_4 concentrations of 448.0 ±

3.0, 1441.8 ± 7.2, and 1718.3 ± 7.2 ppbv, respectively. All standards comprised ambient air mixed with ultra-high purity air (UHP) to achieve the desired methane concentration. UHP air was stripped of CH_4, carbon monoxide (CO), and other gases that may affect GC-IRMS analysis. UHP air was assumed to have the same Kr concentration as that of the ambient air. Standard A was filled at Niwot Ridge, Colorado by the Mountain Research Station of the University of Colorado Boulder. Standards B and C were filled at the University of California Irvine by Dr. Stanley Tyler. All standards were measured against the NOAA/CMDL methane standard scale.

3.1.3. Determining and Applying the Kr Correction

The Kr correction was determined empirically using a graphing method. Kr interference was quantified for each standard as follows:

$$\Delta\,\delta^{13}CH_4 = \delta^{13}CH_{4o} - \delta^{13}CH_{4m} \quad (1)$$

where $\Delta\,\delta^{13}CH_4$ is the Kr interference, $\delta^{13}CH_{4o}$ was measured with the original PSU system, and $\delta^{13}CH_{4m}$ was measured with the modified PSU system. Because each standard was measured only one time, an uncertainty calculation was not possible. Thus, an uncertainty of ± 0.3‰ was assigned to each measurement based on previous PSU studies[4,24].

The Kr interference for each standard was plotted against the inverse of its respective methane concentration. For each standard, $1/[CH_4]$ was interpolated from $[CH_4]$ records from the literature[7–10]. The slope of the best-fit line through the data defined PSU's Kr correction as a function of $1/[CH_4]$. This correction was applied to raw $\delta^{13}CH_4$ data as follows:

$$\delta^{13}CH_{4corrSA} = \delta^{13}CH_{4measSA} - K/[CH_4]_{SA} \quad (2)$$

where $\delta^{13}CH_{4corrSA}$ is the corrected sample value, $\delta^{13}CH_{4measSA}$ is the measured sample value, $[CH_4]_{SA}$ is the methane concentration of the sample, and K is the Kr correction.

Previous datasets had been corrected for an instrument offset (IO), but this correction did not consider Kr interference. The IO was defined as the difference between the measured $\delta^{13}CH_4$ of standard C ($\delta^{13}CH_{4measC}$) and its known value (A), found by:

$$IO = \delta^{13}CH_{4measC} - A \quad (3)$$

These measurements were made 5-10 times each week and applied daily. To account for Kr interference, a new instrument offset (IO_{new}) was calculated as follows:

$$IO_{new} = \delta^{13}CH_{4measC} - A - K/[CH_4]_C \quad (4)$$

where $[CH_4]_C$ is the methane concentration of standard C. Equations (2), (3), and (4) were combined for the final correction:

$$\delta^{13}CH_{4corrSA} = \delta^{13}CH_{4measSA} + K(1/[CH_4]_C - 1/[CH_4]_{SA}) \quad (5)$$

where $\delta^{13}CH_{4corrSA}$ is the final measurement, and $K(1/[CH_4]_C - 1/[CH_4]_{SA})$ is the total applied Kr correction.

3.2. Modeling Methods

A simple two box model was used to constrain source emissions in each hemisphere. The model was based on that of Tans[20] and included the Northern Hemisphere (NH) and Southern Hemisphere (SH) as two perfectly mixed boxes. To remain consistent with previous studies, the interhemispheric exchange rate (k) and lifetime of methane (λ) were held constant at 1 and 7.6 $years^{-1}$, respectively[2,3,16,26]. For a full-constrained inversion, sources were consolidated into two categories: BMB and biogenic, which are the primary levers for the atmospheric $\delta^{13}CH_4$ signal. Each category was assigned $\delta^{13}CH_4$ signatures from Mischler et al.[3] and the references therein[14,16,18,26] (Table 1). Similarly, methane sinks were consolidated into one term[19]. To

account for kinetic isotope effects during sink processes, a fractionation factor (α) of 0.9946 was assigned for $k(^{13}CH_4)/k(^{12}CH_4)$ based on Mischler et al.[3] and the references therein[19,27–29] (Table 2).

Table 1. Source signatures used in two-box model. Modified from Mischler et al.[3].

Source	**$\delta^{13}CH_4$ (‰)**
Biomass Burning	-23.6 ± 2[18]
*Biogenic	-58 ± 7[13,14,16,26]
**Geologic	-38 ± 7[13,14]

* Weighted average of natural and agricultural sources in Mischler et al.[3].
** Not included as source for complete inversion but will contributed to total emissions.

Table 2. Sink kinetic isotope effect fractionation factors (α) used in two-box model. Modified from Mischler et al.[3].

Sink	**Relative Contribution (%)**[19]	**α_{13C} $k(^{13}CH_4)/k(^{12}CH_4)$**
Troposphere	88 ± 2.9	0.9961 ± 0.0004[27]
Stratosphere	7 ± 2.6	0.9847 ± 0.0047[28]
Soils	5 ± 3.4	0.9824 ± 0.0032[29]
Total	----	0.9946 ± 0.0008

Methane sources were constrained using $[CH_4]$ data from the literature[6–10], interpolar gradient (IPG) data from the literature[7], and $\delta^{13}CH_4$ data from each study. Mass balance equations for $[CH_4]$ and $\delta^{13}CH_4$ were written to solve for source emissions in each hemisphere. Sapart et al.[2] and Sowers[4] data were used to estimate emissions in the NH, and Mischler et al.[3] data were used to estimate emissions in the SH. The system of equations was solved with one year time steps over the range of each dataset.

CHAPTER FOUR

Results

4.1. Analytical Results

The modified CF-IRMS system effectively separated Kr from the CH_4 sample. In the original system, the Kr peak eluted under the methane peak, enriching $\delta^{13}CH_4$ measurements by up to ~0.5‰. With the additional 8 m of PLOT column, the Kr peak eluted ~15 seconds before the methane peak (Fig. 5).

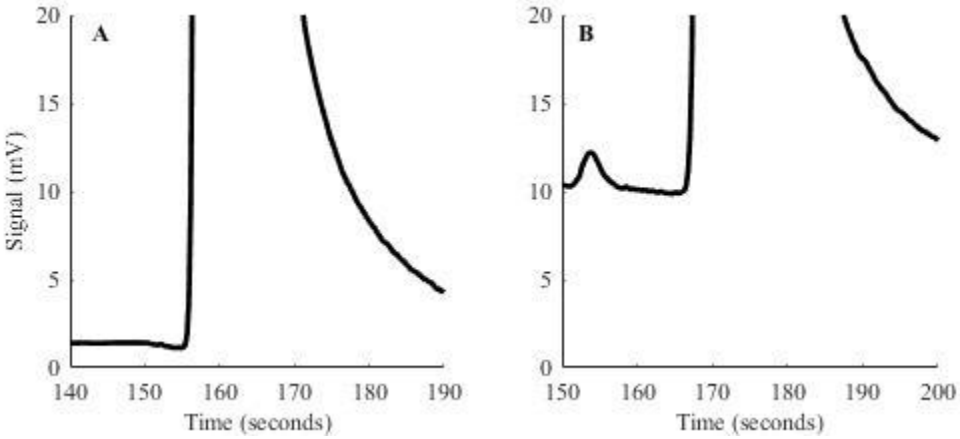

Figure 5. Chromatographs of Standard C's CH_4 peak with PSU's original (A) and modified (B) CF-IRMS system. In the original system, the Kr peak eluted under the methane peak. In the modified system, the Kr peak preceded the CH_4 peak by ~15 seconds.

The best-fit line for the Kr correction, determined with MATLAB's polyfit function, was

$$\Delta\ \delta^{13}CH_4 = 313*x + 0.28 \qquad (6)$$

where 313 was the Kr correction as a function of $1/[CH_4]$. The intercept was a constant offset in $\delta^{13}CH_4$ data and was not included in the correction. The uncertainty in the Kr correction was ± 346, found by fitting the minimum and maximum slope within the analytical uncertainty (Fig. 6).

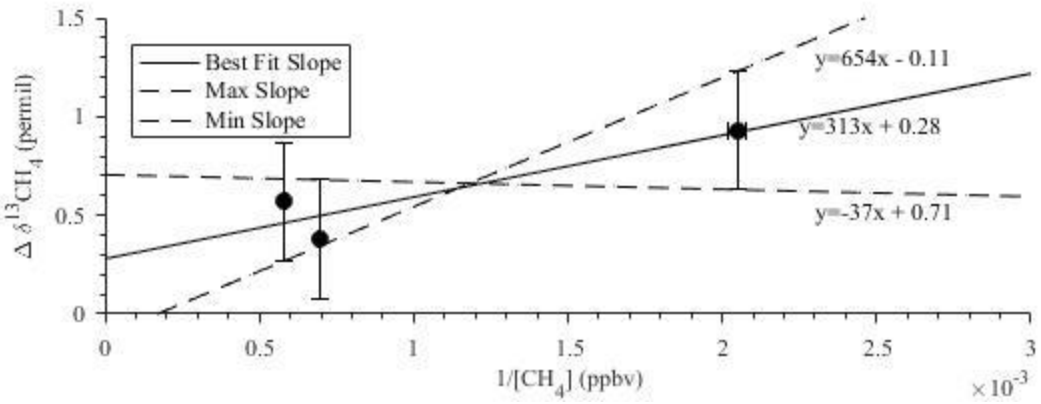

Figure 6. PSU's Kr correction as a function of 1/[CH_4]. The uncertainty in the Kr correction was ± 346, found by fitting the minimum and maximum slopes within the analytical uncertainty.

Over the past 11.3ky, [CH_4] ranged between ~500 and 1680 ppbv, and the applied correction ranged between 0 and -0.4 ± 0.4‰ (Fig. 7). The smallest corrections were for data over the past ~200 years, causing uncorrected and corrected $\delta^{13}CH_4$ records to converge (Fig. 8).

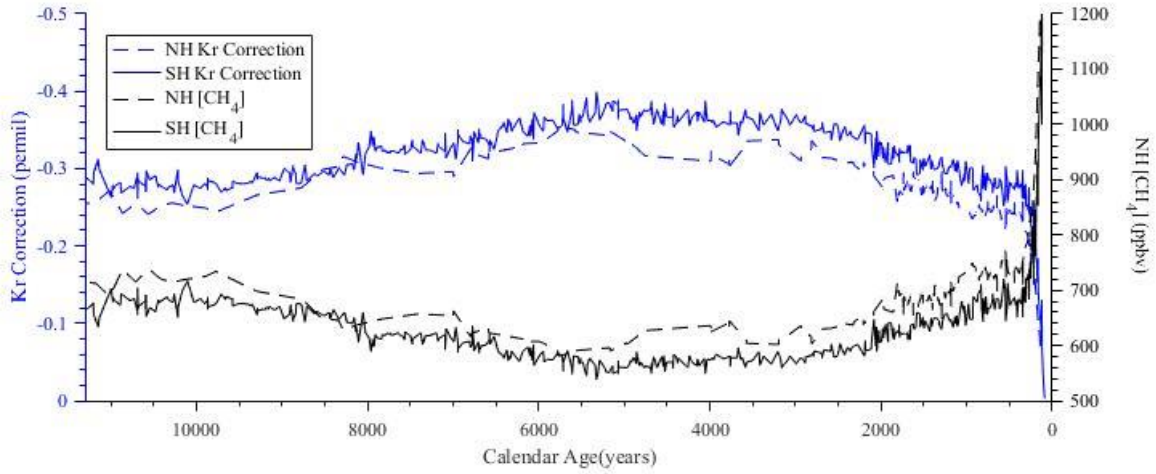

Figure 7. Correlation of the Kr correction and atmospheric [CH_4] over the Holocene. As [CH_4] increased, the Kr correction decreased and vice versa.

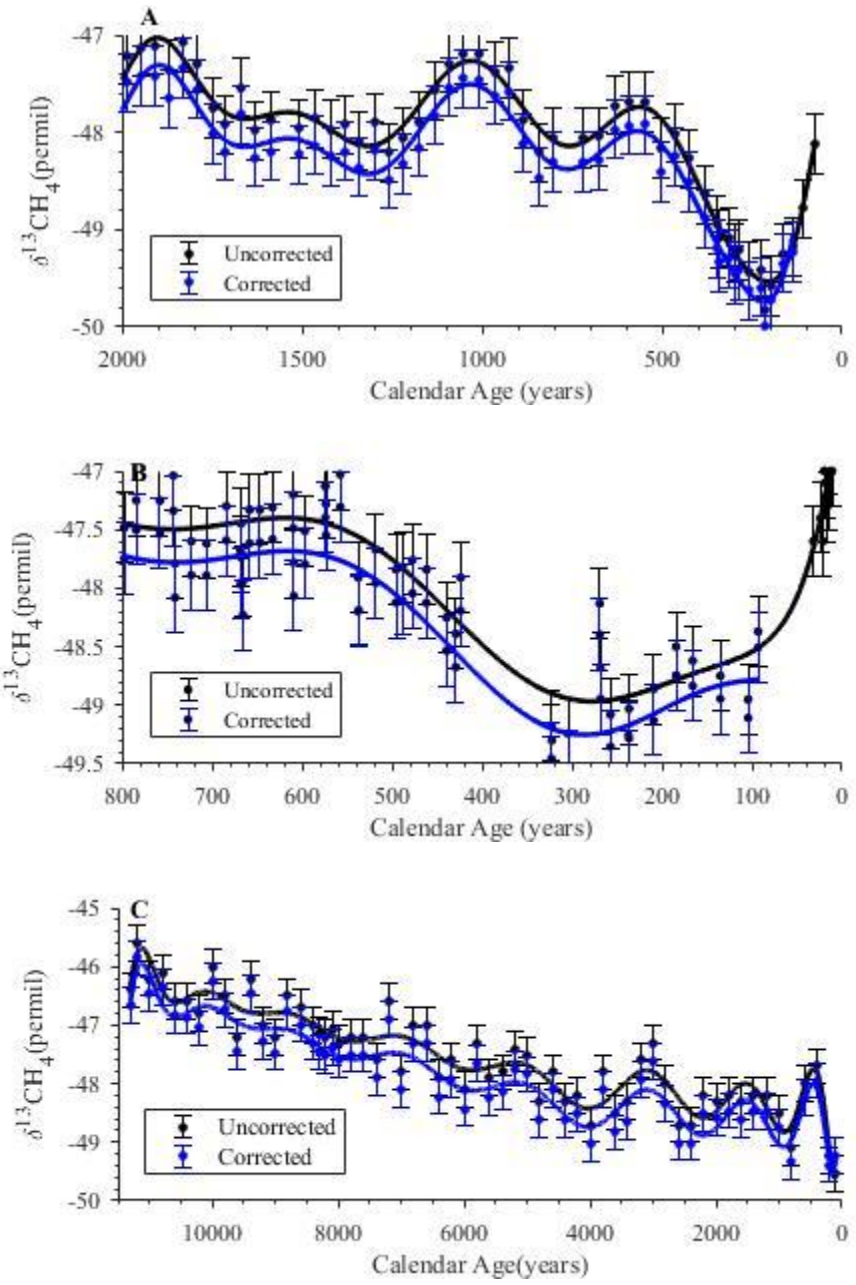

Figure 8. Original and corrected $\delta^{13}CH_4$ records from Sapart et al.[2] (A), Mischler et al.[3] (B), and Sowers[4] (C). In all studies, the corrected and uncorrected data began to converge as time moved toward the present, and [CH_4] continued to rise.

4.2. Model Results

The Kr correction reduced estimated emissions from biomass burning and increased estimated emissions from biogenic sources by the same amount, relative to the uncorrected datasets. Until 200 years before present (ybp), the correction uncertainty was ~0.2% of the mass (Tg) of methane in the atmosphere. Between 200 ybp and present, the correction continued to decrease as [CH_4] increased. The largest correction for the Sapart et al.'s[2] and Sowers'[4] records (NH) was 1.5 ± 1.6 Tg/year during the mid-Holocene (Fig. 9 and 10). The largest correction in Mischler et al.'s[3] record (SH) was 0.4 ± 0.5 Tg/year (Fig. 11). Over the past 200 years, the Kr correction decreased to 0.5 ± 0.6 Tg/year in the NH, and 0.1 ± 0.1 Tg/year in the SH (Fig. 9). In all cases, the flux correction was within the ± 8.6 Tg/year uncertainty envelope of the flux calculation.

Modeled source fluxes agreed with values from the literature[13,17,30–33] (Table 3). All records showed an increase in both BMB and biogenic methane emissions after ~1750 CE (Fig. 9-11). In the Sapart et al.[2] record, for example, BMB emissions rose by ~25 Tg/year, and biogenic emission rose by ~60 Tg/year.

Table 3. Literature estimates of methane source emissions and their distribution between hemispheres. Modified from Mischler et al.[3].

Methane Source	**Estimate Global Emissions Range (Tg/year)**	**NH (%)**	**SH (%)**
Biomass Burning	5-45	44	56
*Biogenic	60-292	78	22
**Geologic	5-53	90	10

*Weighted average of natural and agricultural sources from Mischler et al.[3].
**Not included as source for complete inversion but will contribute to total emissions.

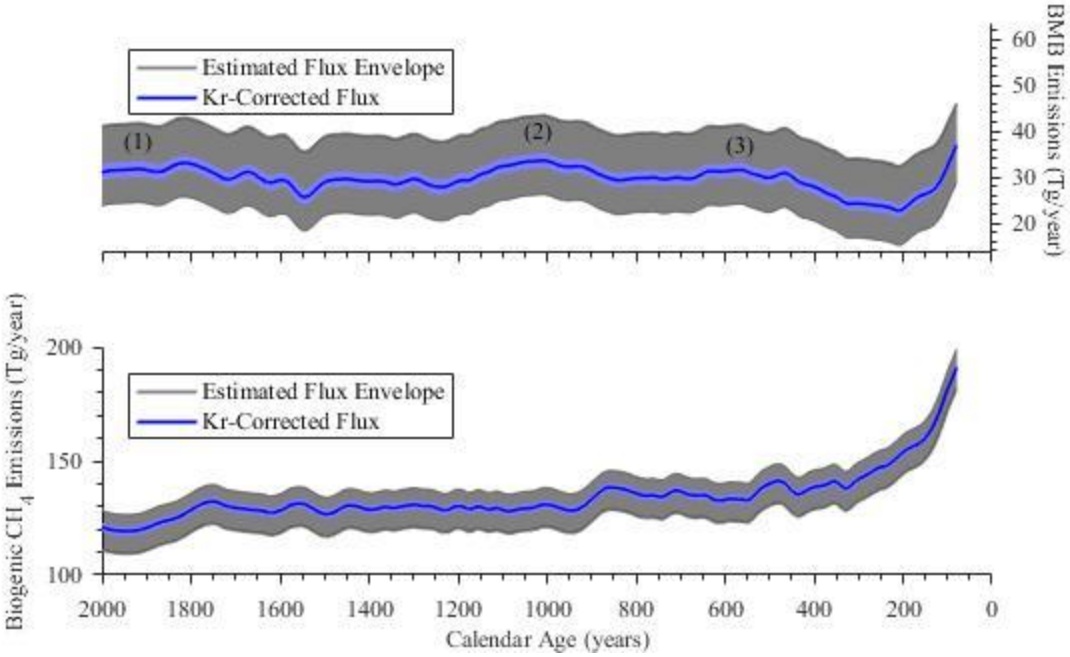

Figure 9. Estimated BMB and biogenic methane emissions in the Northern Hemisphere from Sapart et al.'s[2] original $\delta^{13}CH_4$ data (black), and the corresponding Kr flux correction (blue). The uncertainty envelope of the emissions estimate (grey) was ± 8.6 Tg/year, and the maximum flux correction was 1.5 ± 1.6 Tg/year. As such, the Kr-corrected flux is indistinguishable from the original record. The two-source model reproduced the three source shifts that Sapart et al.[2] identified in their original study (1-3).

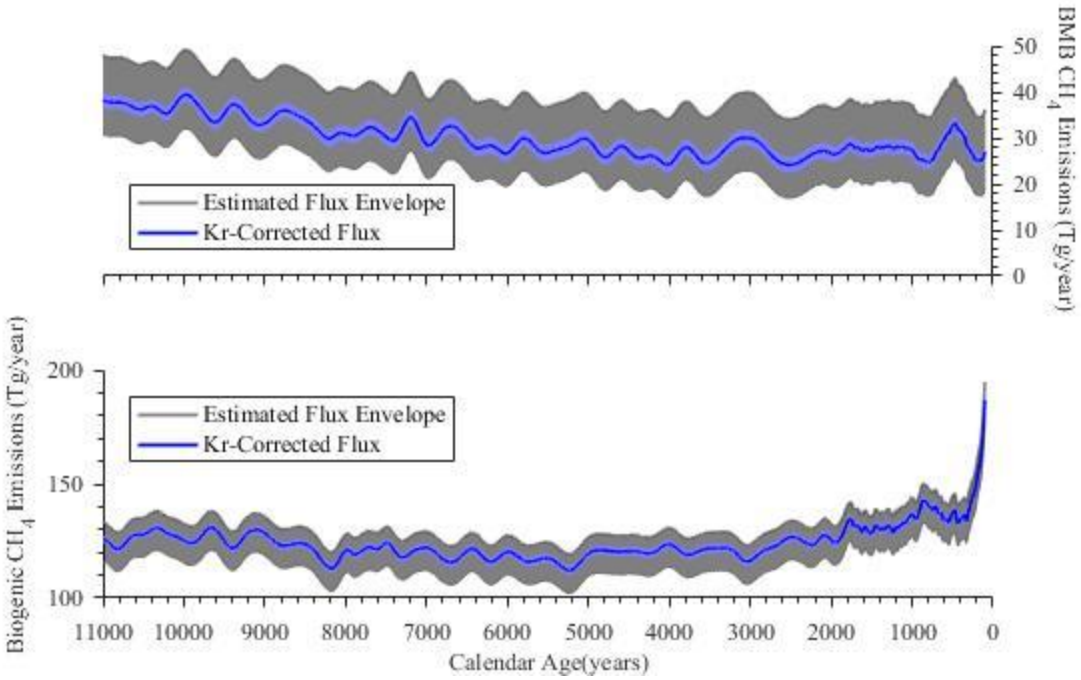

Figure 10. Estimated BMB and biogenic methane emissions in the Northern Hemisphere from Sowers'[4] original $\delta^{13}CH_4$ data (black), and the corresponding Kr flux correction (blue). The uncertainty envelope of the emissions estimate (grey) was ± 8.6 Tg/year, and the maximum flux correction was 1.5 ± 1.6 Tg/year. As such, the Kr-corrected flux is indistinguishable from the original record.

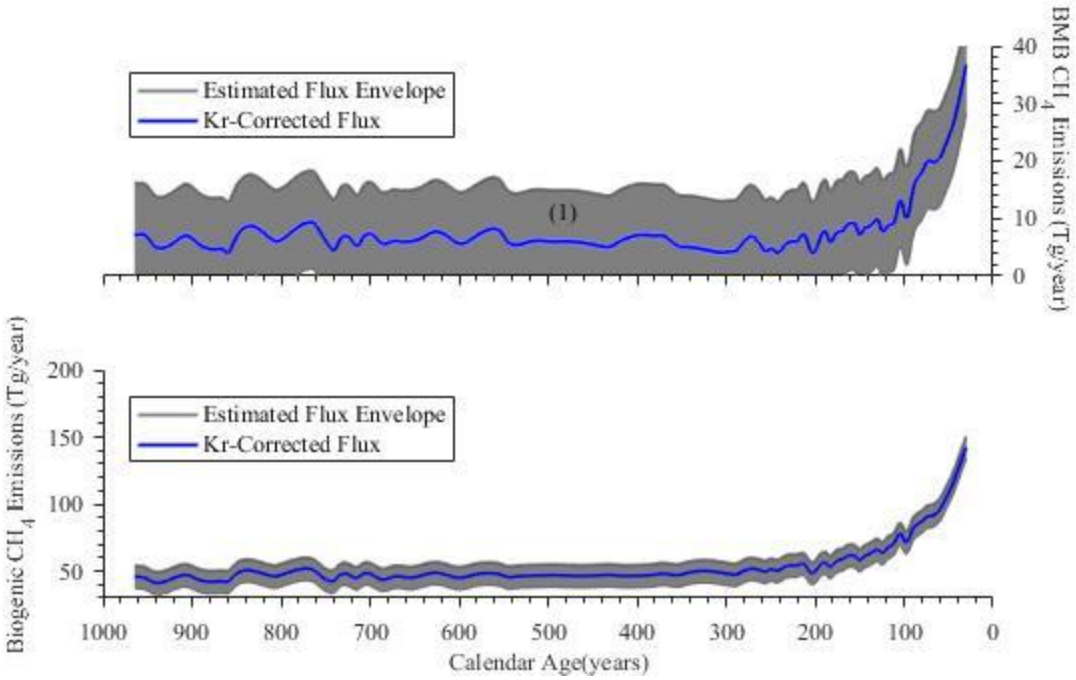

Figure 11. Estimated BMB and biogenic methane emissions in the Southern Hemisphere from Mischler et al.'s[3] original $\delta^{13}CH_4$ data (black), and the corresponding Kr flux correction (blue). The uncertainty envelope of the emission estimate (grey) was ± 8.6 Tg/year, and the maximum flux correction was 0.4 ± 0.5 Tg/year. As such, the Kr-corrected flux was indistinguishable from the original record. The two-box model reproduced the drop in BMB emissions that Mischler et al.[3] linked to European contact with the Americas (1).

CHAPTER 5

Discussion

5.1. Analytical Discussion

The modified CF-IRMS system more than tripled the separation time between the Kr and CH_4 peaks. Schmitt et al.[1] found a similar separation time (16 seconds) for the Bern system when they held the pre-combustion GC column at 5°C. This degree of separation removed Kr interference from $\delta^{13}CH_4$ measurements. Thus, the PSU modification was a success. Further, PSU's Kr correction was indistinguishable from the AWI correction within the combined errors[1]. Both labs had similar analytical systems, so a similar correction was expected.

Despite this success, the graphing technique was not the ideal method to quantify the Kr correction. We conducted this study five years after Sapart et al.[2], and the instrument likely drifted over time. Also, instrument settings changed after the original $\delta^{13}CH_4$ analyses. For example, we reconfigured the IRMS to dual inlet mode and had to reset it to CF mode for the Kr measurements. Because of these alterations, the determined Kr correction was slightly different than it was during the $\delta^{13}CH_4$ measurements for Sapart et al.[2], Mischler et al.[3], and Sowers[4]. Further, the graphing method has greater uncertainty than other correction techniques, such as a time series correction[1]. However, we did not have the raw beam data to complete this correction. Also, the final flux correction was small compared to the total uncertainty, so slight changes in the Kr correction would not have a great effect. Additional measurements would further constrain the calibration curve to reduce the correction uncertainty.

5.2. Model Discussion

Overall, the Kr flux correction ranged from 0.4 ± 0.5 to 1.5 ± 1.6 Tg/year, which fell within the ± 8.6 Tg/year uncertainty envelope of the total flux. This uncertainty was comparable with that of the model used by Sapart et al.[2]. Therefore, PSU's Kr correction did not significantly affect the methane budgets of Sapart et al.[2], Mischler et al.[3], and Sowers[4].

For all records, the model showed a marked increase in reconstructed BMB and biogenic methane emissions after ~1750 CE, which coincided with a > 500 ppbv increase in $[CH_4]$[9,10]. These shifts were caused by rising anthropogenic emissions, particularly growth in industry, fossil fuels, agriculture and ruminants[5]. In the Sapart et al.[2] record, BMB emissions rose by ~25 Tg/year, and biogenic emissions rose by ~60 Tg/year. The ratio of biogenic emissions to BMB emissions fell from ~5:1 to 4:1, which agrees with the 1.5‰ increase in atmospheric $\delta^{13}CH_4$.

Though the model included only two methane sources, it retained large-scale features of the original methane budgets. The updated Sapart et al.[2] budget showed the three source shifts described in the original study (Fig. 9). The new Mischler et al.[3] record also shows lower BMB emissions in the 15th and 16th centuries, which they linked to European contact with the Americas (Fig. 11). Lastly, the Sowers[4] record showed a ~10 Tg/year drop in BMB emissions between 11.3 ka and 4 ka (Fig. 10). This trend aligns with his hypothesis that Arctic lakes ($\delta^{13}CH_4$ -70‰)[21] increased methane emissions in the mid-Holocene. However, Sowers[4] also attributed this shift to an increase in C3 plants ($\delta^{13}CH_4$= ~-25‰) relative to C4 plants ($\delta^{13}CH_4$= ~-16‰)[22]. To capture these finer details, we need to add additional sources to the model. In this study, however, the calculated flux shifts were small relative to the measurement and computational uncertainties. Thus, a simpler model was appropriate.

Though Kr interference did not significantly affect this study, it may be greater in other CF-IRMS systems. As previously noted, the correction at IMAU was 2.38‰ for a sample with a CH_4 concentration of 372 ppb. Because Kr interference is inversely proportional to [CH_4], it impacts some studies more than others. For example, ice cores contain air samples that span numerous glacial/interglacial cycles. In the Last Glacial Maximum (LGM), [CH_4] was as low as ~350 ppb[8], so Kr interference would strongly impact $\delta^{13}CH_4$ measurements. Kr also affects modern air samples with low [CH_4]/Kr, such as samples from the stratosphere. Schmitt et al.[1] highlighted that samples of ocean surface water are also susceptible because Kr is more soluble than CH_4. Lastly, inter-lab calibrations or round robin studies must consider Kr interference because it is not a universal correction.

Kr interference is also more significant during rapid changes in [CH_4]. If [CH_4] is relatively stable (e.g. the mid-Holocene), the Kr correction is almost constant. Thus, the entire $\delta^{13}CH_4$ record moves down by the same amount, but the overall shape of the curve remains the same. This shift alters the overall source allocation, but it does not impact temporal fluctuations in CH_4 emissions within each source. However, during rapid changes in [CH_4] (e.g. the late post-industrial Holocene), the Kr correction changes more over a short period. This variation alters the shape of the $\delta^{13}CH_4$ record, which affects temporal changes in single source emissions. Thus, Kr-corrected methane budgets better reveal trade-offs between methane sources over time, leading to more accurate reconstructions of climate and human activity.

CHAPTER SIX

Conclusion

Methane budgets use atmospheric [CH_4] and $\delta^{13}CH_4$ measurements to constrain methane sources over time. However, Schmitt et al.[1] found that CF-IRMS analysis does not adequately separate Kr from CH_4, which enriches $\delta^{13}CH_4$ measurements by as much as 2.38‰. To correct for this interference at PSU, we added 8 m of PLOT column after the combustion chamber in our preconcentration unit. This additional column separated Kr from the CO_2 sample peak before the sample entered the IRMS. With an empirical graphing technique, we determined a Kr correction for $\delta^{13}CH_4$ data measured at PSU. We then applied this correction to methane budget studies by Sapart et al.[2], Mischler et al.[3], and Sowers[4]. The Kr correction was a function of 1/[CH_4] and, thus, varied over time. For these datasets, PSU's Kr correction ranged from 0 to -0.4 ± 0.4‰ throughout the Holocene. This correction is similar to corrections at AWI and Bern, which have comparable analytical systems as PSU.

We built a simple two-box model to determine if and how the Kr correction affected the work of Sapart et al.[2], Mischler et al.[3], and Sowers[4]. The model used the given isotope data combined with [CH_4] records to constrain BMB and biogenic methane emissions. The uncertainty in the estimated flux was ± 8.6 Tg/year, similar to that of Sapart et al.[2]. A simple, two-source model was appropriate for this study because of the small Kr correction relative to the combined measurement and computational error. We analyzed both the original and corrected data sets and found a maximum flux correction of 1.5 ± 1.6 Tg/year. This shift was within the estimated flux uncertainty and, therefore, indistinguishable from the original data. Though PSU's Kr correction had little effect in this study, it may be greater for other CF-IRMS systems. The correction is most significant for samples with low [CH_4]/Kr and during rapid

changes in [CH_4]. As such, the Kr correction is an important factor in past and future methane budgets.

References

1. Schmitt, J. *et al.* On the interference of Kr during carbon isotope analysis of methane using continuous-flow combustion-isotope ratio mass spectrometry. *Atmos. Meas. Tech.* **6,** 1425–1445 (2013).
2. Sapart, C. J. *et al.* Natural and anthropogenic variations in methane sources during the past two millennia. *Nature* **490,** 85–88 (2013).
3. Mischler, J. A. *et al.* Carbon and hydrogen isotopic composition of methane over the last 1000 years. *Global Biogeochem. Cycles* **23,** (2009).
4. Sowers, T. Atmospheric methane isotope records covering the Holocene period. *Quat. Sci. Rev.* **29,** 213–221 (2010).
5. Blunier, T. *et al.* Atmospheric methane record from Greenland ice core over the last 1000 year. *Geophys. Res. Lett.* **20,** 2219–2222 (1993).
6. Blunier, T., Chappellaz, J., Schwander, J., Stauffer, B. & Raynaud, D. Variations in atmospheric methane concentration during the Holocene epoch. *Nature* **374,** 46–49 (1995).
7. Chappellaz, J. *et al.* Changes in the atmospheric CH4 gradient between Greenland and Antarctica during the Holocene. *J. Geophys. Res.* **102,** 15987–15997 (1997).
8. Loulergue, L. *et al.* Orbital and millennial-scale features of atmospheric CH4 over the past 800,000 years. *Nature* **453,** 383–386 (2008).
9. MacFarling Meure, C. *et al.* Law Dome CO2, CH4 and N2O ice core records extended to 2000 years BP. *Geophys. Res. Lett.* **33,** 2000–2003 (2006).
10. Rhodes, R. H. *et al.* Continuous methane measurements from a late Holocene Greenland ice core: Atmospheric and in-situ signals. *Earth Plan etary Sci. Lett.* **368,** 9–19 (2013).
11. Etheridge, D. M., Steele, L. P., Francey, R. J. & Langenfelds, R. L. Atmospheric methane between 1000 A . D . and present : Evidence of anthropogenic emissions and climatic variability. *J. Geophys. Res.* **103,** 15979–15993 (1998).
12. Allen, D. Attributing Atmospheric Methane to Anthropogenic Emission Sources. *Acc. Chem. Res.* **49,** 1344–1350 (2016).
13. Lassey, K. R., Etheridge, D. M., Lowe, D. C., Smith, a. M. & Ferretti, D. F. Centennial evolution of the atmospheric methane budget: what do the carbon isotopes tell us? *Atmos. Chem. Phys. Discuss.* **6,** 4995–5038 (2007).
14. Quay, P. *et al.* The isotopic composition of atmospheric methane. *Global Biogeochem. Cycles* **13,** 445–461 (1999).
15. Houweling, S., van der Werf, G. R., Goldewijk, K. K., Röckmann, T. & Aben, I. Early anthropogenic CH4 emissions and the variation of CH4 and 13CH4 over the last millennium. *Global Biogeochem. Cycles* **22,** (2008).
16. Ferretti, D. F. *et al.* Unexpected changes to the global methane budget over the past 2000 years. *Science (80-.).* **309,** 1714–1717 (2005).
17. Fischer, H. *et al.* Changing boreal methane sources and constant biomass burning during the last termination. *Nature* **452,** 864–867 (2008).
18. Yamada, K. *et al.* Hydrogen and carbon isotopic measurements of methane from agricultural combustion: Implications for isotopic signatures of global biomass burning sources. *J. Geophys. Res. Atmos.* **111,** 1–12 (2006).
19. Reeburgh, W. S. Global Methane Biogeochemistry. *Treatise Geochemistry Second Ed.* **4,** 65–89 (2004).

20. Tans, P. P. A note of isotopic ratios and the global atmosheric methane budget. *Global Biogeochem. Cycles* **11,** 77–81 (1997).
21. Walter, K. M., Edwards, M. E., Grosse, G., Zimov, A. & Chapin III, F. S. Thermokarst Lakes as a Source of Atmospheric CH4 during the last Deglaciation. *Science (80-.).* **318,** 633–636 (2007).
22. Farquhar, G. D., Enleringer, J. R. & Hubick, K. T. Carbon Isotope Discrimination and Photosynthesis. *Annu. Rev. Plant Physiol. Plant Mol. Biol.* **40,** 503–537 (1989).
23. Milkov, A. V. Molecular and stable isotope compositions of natural gas hydrates: A revised global dataset and basic interpretations in the context of geological settings. *Org. Geochem.* **36,** 681–702 (2005).
24. Sowers, T. *et al.* Records of the δ13C of atmospheric CH4 over the last 2 centuries as recorded in Antarctic snow and ice. *Global Biogeochem. Cycles* **19,** 1–12 (2005).
25. Schaefer, H. *et al.* Ice Record of d13C for Atmospheric CH4 Across the Younger Dryas-Preboreal Transition. *Science (80-.).* **313,** 1109–1112 (2006).
26. Houweling, S., Dentener, F. & Lelieveld, J. Simulation of preindustrial atmospheric methane to constrain the global source strength of natural wetlands. *J. Geophys. Res.* **105,** 17,243-17255 (2000).
27. Saueressig, G., Crowley, J. N., Bergamaschi, P., Brenninkmeijer, C. A. M. & Fischer, H. Carbon 13 and D kinetic isotope effects in the reactions of CH4 with O(1D) and OH: New laboratory measurements and their implications for the isotopic composition of stratoshperic methane. *J. Geophys. Res.* **106,** 23127–23138 (2001).
28. Rice, a. L. Carbon and hydrogen isotopic compositions of stratospheric methane: 1. High-precision observations from the NASA ER-2 aircraft. *J. Geophys. Res.* **108,** 4460 (2003).
29. Mahieu, K., Visscher, A. D., Vanrolleghem, P. A. & Cleemput, O. Van. Carbon and hydrogen isotope fractionation by microbial methane oxidation: Improved determination. *Waste Manag.* **26,** 389–398 (2006).
30. Marik, T. Atmospheric d13C and dD measurements to balance the global methane budget, Ph.D. thesis. (Max Plank Institute, 1998).
31. Ruddiman, W. F. The Anthropogenic Greenhous Era Began Thousands of Years Ago. *Clim. Change* **61,** 261–293 (2003).
32. Etiope, G., Lassey, K. R., Klusman, R. W. & Boschi, E. Reappraisal of the fossil methane budget and related emission from geologic sources. *Geophys. Res. Lett.* **35,** (2008).
33. Wuebbles, D. J. & Hayhoe, K. Atmospheric methane and global change. *Earth-Sci. Rev.* **57,** 177–210 (2002).

APPENDIX

Matlab Code

We used three versions of a basic two-box model. The Matlab code for the Sapart et al.[2] dataset follow below.

```
%%%%%%%%%%%LOAD DATA%%%%%%%%%%%%%%%%%%%%%%%%%
SHdata=csvread('SHmethane.csv');
NHdata=csvread('NHmethane.csv');
SAdata=csvread('SAPART.csv');

%%%%%%%%%%CONSTANTS%%%%%%%%%%%%%%%%%%%%%%%%%%
smooth=0.005;
Tg=1.18; %conversion from ppb to Tg
std13=0.0112372; %VPDB
NA12=0.989;  %natural abundance C12

%%%%%%%%%%SOURCE R VALUES%%%%%%%%%%%%%%%%%%%%
deltaC1=-23.6;  %%%BMB
deltaC2=-58.0;  %%%%biogenic
R131=((deltaC1/1000+1)*std13)*NA12;
R132=((deltaC2/1000+1)*std13)*NA12;

%%%%%%%%%%EXTRACT METHANE DATA%%%%%%%%%%%%%%%%
NHyear=NHdata(:,1);
NHppb=NHdata(:,2);
NHtg=NHppb*Tg;

SHyear=SHdata(:,1);
SHppb=SHdata(:,2);
SHtg=SHppb*Tg;

    %smooth
    NHppbcurve=csaps(NHyear,NHppb,smooth,NHyear);
    NHppbpp=csaps(NHyear,NHppbcurve,smooth);
    NHppbpd=fnder(NHppbpp);
    NHtgcurve=csaps(NHyear,NHtg,smooth,NHyear);
    NHtgpp=csaps(NHyear,NHtgcurve,smooth);
    NHtgpd=fnder(NHtgpp);

    SHppbcurve=csaps(SHyear,SHppb,smooth,SHyear);
    SHppbpp=csaps(SHyear,SHppbcurve,smooth);
    SHppbpd=fnder(SHppbpp);
    SHtgcurve=csaps(SHyear,SHtg,smooth, SHyear);
    SHtgpp=csaps(SHyear,SHtgcurve,smooth);
    SHtgpd=fnder(SHtgpp);

%%%%%%%%%%EXTRACT SAPART DATA%%%%%%%%%%%%%%%%
SAyear=SAdata(:,1);
SA13=SAdata(:,2);
SA13R=((SA13/1000+1)*std13)*NA12;
```

```
    %smooth sapart
    SA13curve=csaps(SAyear,SA13,smooth,SAyear);
    SA13pp=csaps(SAyear,SA13curve,smooth);
    SA13Rcurve=csaps(SAyear,SA13R,smooth,SAyear);
    SA13Rpp=csaps(SAyear,SA13Rcurve,smooth);

%%%%%%%%%%CALCULATE KRYPTON CORRECTION%%%%%%%%%
stdmeas=-46.87;
stdassigned=-47.1;
stdch4ppb=1718;
Kbest=313;%over uncertainty range
Kupper=654;
Klower=-37;
IOcorrectionbest=Kbest/stdch4ppb;%(stdmeas-stdassigned)-(stdmeas-stdassigned-
Kbest/stdch4ppbv);
IOcorrectionupper=Kupper/stdch4ppb;
IOcorrectionlower=Klower/stdch4ppb;
Samplecorrectionbest=Kbest./ppval(NHppbpp,SAyear);
Samplecorrectionupper=Kupper./ppval(NHppbpp,SAyear);
Samplecorrectionlower=Klower./ppval(NHppbpp,SAyear);
%total correction
KCbest=IOcorrectionbest-Samplecorrectionbest;
KCupper=IOcorrectionupper-Samplecorrectionupper;
KClower=IOcorrectionlower-Samplecorrectionlower;

%%%%%%%%%%APPLY KRYPTON CORRECTION%%%%%%%%%%
%best fit
SA13bestcorrected=SA13+KCbest;
SA13Rbestcorrected=(SA13bestcorrected/1000+1)*std13*NA12;
    %smooth
    SA13Rbestcorrectedcurve=csaps(SAyear,SA13Rbestcorrected,smooth,SAyear);
    SA13Rbestcorrectedpp=csaps(SAyear,SA13Rbestcorrectedcurve,smooth);

%upper fit
SA13uppercorrected=SA13+KCupper;
SA13Ruppercorrected=(SA13uppercorrected/1000+1)*std13*NA12;
    %smooth
    SA13Ruppercorrectedcurve=csaps(SAyear,SA13Ruppercorrected,smooth,SAyear);
    SA13Ruppercorrectedpp=csaps(SAyear,SA13Ruppercorrectedcurve,smooth);

%lower fit
SA13lowercorrected=SA13+KClower;
SA13Rlowercorrected=(SA13lowercorrected/1000+1)*std13*NA12;
    %smooth
    SA13Rlowercorrectedcurve=csaps(SAyear,SA13Rlowercorrected,smooth,SAyear);
    SA13Rlowercorrectedpp=csaps(SAyear,SA13Rlowercorrectedcurve,smooth);

%%%%%%%%%%%%%%MODEL for Q1 and Q2%%%%%%%%%%%%%%%%%%
lambda=1/7.6;
alpha=0.9946;
k=1;
IPG=44*Tg; %from lit - Average Holocene
mint=80; %minimum age in all datasets
maxt=SAyear(55);%maximum age in all datasets
x=mint:maxt;
```

```
for t=SAyear(1):1:SAyear(55);

 %%%estimated uncorrected flux
    Qt=fnval(NHtgpd,t)+lambda*ppval(NHtgpp,t)+k*IPG;

Q1=(ppval(SA13Rpp,t)*(fnval(NHtgpd,t)+lambda*alpha*ppval(NHtgpp,t)+k*IPG)-
Qt*R132)/(R131-R132);
    Q2=Qt-Q1;
    Q1out(t)=Q1;
    Q2out(t)=Q2;

        %uncertainty in estimated flux
        fluxuncertainty=8.6; %%%calculated from analytical and lit data
        %upper/lowerbounds of Q1 and Q1
        upperQ1=Q1+fluxuncertainty;
        upperQ1out(t)=upperQ1;
        upperQ2=Q2+fluxuncertainty;
        upperQ2out(t)=upperQ2;
        lowerQ1=Q1-fluxuncertainty;
        lowerQ1out(t)=lowerQ1;
        lowerQ2=Q2-fluxuncertainty;
        lowerQ2out(t)=lowerQ2;

    %estimated corrected flux
    %best

Q1bestcorrected=(ppval(SA13Rbestcorrectedpp,t)*(fnval(NHtgpd,t)+lambda*alpha*
ppval(NHtgpp,t)+k*IPG)-Qt*R132)/(R131-R132);
    Q2bestcorrected=Qt-Q1bestcorrected;
    Q1bestcorrectedout(t)=Q1bestcorrected;
    Q2bestcorrectedout(t)=Q2bestcorrected;

    %upper

Q1uppercorrected=(ppval(SA13Ruppercorrectedpp,t)*(fnval(NHtgpd,t)+lambda*alph
a*ppval(NHtgpp,t)+k*IPG)-Qt*R132)/(R131-R132);
    Q2uppercorrected=Qt-Q1uppercorrected;
    Q1uppercorrectedout(t)=Q1uppercorrected;
    Q2uppercorrectedout(t)=Q2uppercorrected;

    %lower

Q1lowercorrected=(ppval(SA13Rlowercorrectedpp,t)*(fnval(NHtgpd,t)+lambda*alph
a*ppval(NHtgpp,t)+k*IPG)-Qt*R132)/(R131-R132);
    Q2lowercorrected=Qt-Q1lowercorrected;
    Q1lowercorrectedout(t)=Q1lowercorrected;
    Q2lowercorrectedout(t)=Q2lowercorrected;

    %%%%%%%size of flux correction
      %best
    Q1bestfluxcorrection=Q1bestcorrected-Q1;
    Q1bestfluxcorrectionout(t)=Q1bestfluxcorrection;
    Q2bestfluxcorrection=-Q1bestfluxcorrection;
    Q2bestfluxcorrectionout(t)=Q2bestfluxcorrection;
```

```
      %upper
    Q1upperfluxcorrection=Q1uppercorrected-Q1;
    Q1upperfluxcorrectionout(t)=Q1upperfluxcorrection;
    Q2upperfluxcorrection=-Q1upperfluxcorrection;
    Q2upperfluxcorrectionout(t)=Q2upperfluxcorrection;

      %lower
    Q1lowerfluxcorrection=Q1lowercorrected-Q1;
    Q1lowerfluxcorrectionout(t)=Q1lowerfluxcorrection;
    Q2lowerfluxcorrection=-Q1lowerfluxcorrection;
    Q2lowerfluxcorrectionout(t)=Q2lowerfluxcorrection;

end

%%%%%%%%%%%%%%%%%%PLOT SOURCE ALLOCATIONS%%%%%%%%%%%%%%%

subplot(2,1,1) %BMB
u=[.5 .5 1];
g=[.5 .5 .5];

h(1)=plot(x,upperQ1out(x),'Color',g,'LineWidth',1.25,'DisplayName','Estimated
Flux Envelope');
hold on
plot(x,lowerQ1out(x),'Color',g);
plot(x,Q1lowercorrectedout(x),'Color',u);
plot(x,Q1uppercorrectedout(x),'Color',u);

    [ph,msg]=jbfill(x,upperQ1out(x),lowerQ1out(x),'k',g,0,.5);
    [ph,msg]=jbfill(x,Q1lowercorrectedout(x),Q1uppercorrectedout(x),u,u,0,
1);

h(2)=plot(x,Q1bestcorrectedout(x),'b','LineWidth',1.25,'DisplayName','Kr-
Corrected Flux');
hold off


subplot(2,1,2) %biogenic

o(1)=plot(x,lowerQ2out(x),'Color',g,'Linewidth',1.25,'DisplayName','Estimated
Flux Envelope');
hold on
plot(x,upperQ2out(x),'Color',g);
plot(x,Q2uppercorrectedout(x),'Color',u);
plot(x,Q2lowercorrectedout(x),'Color',u);

    [ph,msg]=jbfill(x,upperQ2out(x),lowerQ2out(x),'k',g,0, .5);
    [ph,msg]=jbfill(x,Q2uppercorrectedout(x),Q2lowercorrectedout(x),u,u,0,1);

o(2)=plot(x,Q2bestcorrectedout(x),'b','LineWidth',1.25,'DisplayName','Kr-
Corrected Flux');
hold off
```